Single-volume dual-channel acousto-optical tunable filter

ALEXANDER MACHIKHIN,[1,2] VLADISLAV BATSHEV,[1,3,*] VITOLD POZHAR,[1,3] AND ALEXANDER NAUMOV,[1]

[1]*Laboratory of acousto-optic spectroscopy, Scientific and Technological Center of Unique Instrumentation, Russian Academy of Sciences, 15 Butlerova str., Moscow 117342, Russia*
[2]*Department of Electrical Engineering and Introscopy, Institute of Automatics and Computer Engineering, National Research University "Moscow Power Engineering University", 14 Krasnokazarmennaya str., Moscow 111250, Russia*
[3]*Department of Radioelectronics and Laser Technologies, Bauman Moscow State Technical University, 5 2-ya Baumanskaya str., Moscow 105005, Russia*
**batshev@bmstu.ru*

Abstract: In this paper, we present a novel approach to spectral stereoscopic imaging. It is based on simultaneous spectral filtration of two light beams with a tunable acousto-optical filter (AOTF) of original design. It does not require large crystals and complicated optical relay systems, because two beams diffract in the same volume of the crystal medium but at different angles. We show that this geometry can be composed of a common-type AO cell and two triangular prisms of the same material. We derive equations, which specify the prism angles ensuring the necessary orientation of beams trajectories inside the crystal medium as well as parallel propagation of input and output beams. Some angles were additionally optimized for aberrations minimization by means of ray-tracing simulation. Experimental testing demonstrates rather high quality of spectral images, which is necessary for stereoscopic reconstruction procedure. The proposed approach makes possible development of spectral stereo-imaging components based on different types of previously developed AOTFs.

1. Introduction

Spectral imaging allows registration of spatio-spectral data cube $I(x,y,\lambda)$, i.e. obtaining the spectrum $I(\lambda)$ for each pixel x,y in the image of the inspected object. This technique is widely used for contrast visualization and pattern recognition as well as for spectral measurements [1-3]. Spectral imaging becomes even more effective when it is performed simultaneously with quantitative characterization of 3D shape $z(x,y)$ of the inspected object. In this case, one can analyze the distribution of spectral properties $I(\lambda)$ over the relief of the surface $z(x,y)$ [4-6]. That is why, such 3D imaging spectroscopy systems are of particular interest.

To cover a wide spectral range continuously instead of spaced spectral bands, one needs a tunable narrowband filter. A pair of spectral imagers $I_i(x,y,\lambda)$ enables stereoscopic shape reconstruction $I(x,y,z,\lambda)$ using conventional machine vision techniques [7,8].

AOTF is one of the most promising spectral elements for 3D spectral imaging. It provides high spectral (up to 0.1 nm) and spatial (up to 1000×1000 resolved elements) resolution, fast (less than 10 μs) and precise arbitrary spectral addressing in the ultraviolet, visible and infrared ranges, capability to form and modulate optical transfer function, compactness and low power consumption, absence of moving elements, programmability [9,10]. Imaging AOTFs nowadays have numerous applications in spectroscopy, especially for spectral imaging of physical, chemical and other properties of the inspected objects using the characteristic wavelengths. Due to a well-developed technology, AOTFs may be compact and PC-controlled modules, ready to be integrated into many existing optical schemes. Proper

AO crystal choice, accurate AOTF design and precise optical coupling provide high-throughput and distortion-free imaging [11].

To implement AOTF-based 3D stereoscopic imaging, it is necessary either to use two identical AO spectral imagers [12] or to provide simultaneous effective diffraction of two image-carrying beams [13-16]. In the first case, the system suffers from oversizes, mechanical instability, needs for precise synchronization and for spatio-spectral calibration of stereo channels [12]. In the second case, two alternatives are possible: (1) to transmit two parallel beams or (2) to use the same working volume for beams diffracting under very different angular conditions [14,15] (Fig. 1b). Consequently, option 1 requires a massive large-size crystal, while option 2 requires a tricky crystal shape. For a large-size AOTF, divergence and attenuation of ultrasonic wave may lead to significant difference of image distortions between two channels and, therefore, non-identical conditions of AO interaction of stereoscopic beams. Tricky crystal shape is cost-ineffective and does not suit for a serial production. Another issue preventing this type of AOTF-based 3D spectral imaging technique from mass use is non-parallel propagation of incident and filtered beams, i.e. the necessity of a complicated optical relay system [17]. All these factors degrade the image quality and, therefore, inevitably lead to the distortion of reconstructed 3D image (Fig. 1b).

Fig. 1b illustrates a concept of desirable AOTF-based 3D spectral imaging system, which should be close to conventional AO spectral imagers (Fig. 1a) in terms of practical advantages: single small-size AO crystal, robust and cost-effective design, easy control of the selected wavelength range, minimized image aberrations.

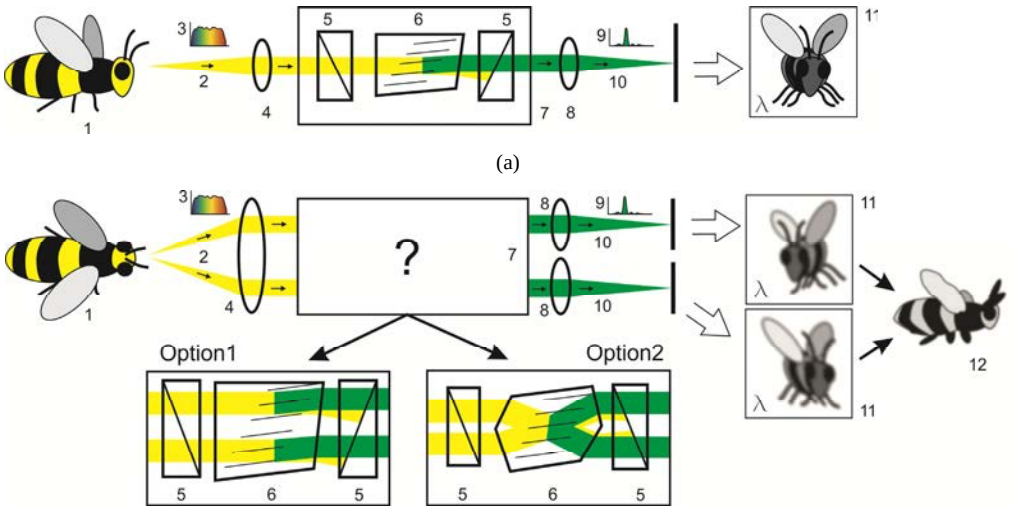

Fig. 1. Concepts of ordinary (a) and stereoscopic (b) AOTF-based spectral imaging system.
1 – inspected object; 2, 10 – input and output beams of the particular point of the object;
3 – input beam spectrum; 4, 8 – input and output lenses; 5 – polarizers; 6 – AO cells;
7 – AOTFs of different configurations; 9 – spectral band selected by AOTF;
11 – detected images; 12 – stereo-image reconstructed.

In this paper, we present a novel approach to dual-channel AOTF design, which is free from the most of known drawbacks. We propose to apply a conventional imaging AO cell with two triangular prisms attached to its faces. Below, we derive equations necessary for prisms design and confirm the effectiveness of this approach experimentally.

2. Technique

The proposed technique is illustrated by Fig. 2a. AOTF operates in wide-aperture mode (non-critical phase matching, Fig. 2b), which is necessary for image filtration [10-16]. In the first channel, AOTF transmits wide-band light B1 as usual. First, the incident beam $\mathbf{k1_i}$ is extraordinary (*e*) polarized by the input polarizer POL1. Then it diffracts inside AO cell AOC by ultrasonic wave (**q**) generated with piezotransducer. Diffracted beam $\mathbf{k1_d}$ is polarized ordinary (*o*), so it transmits through the output polarizer POL2 crossed with respect to POL1, while the undiffracted beam is stopped.

The second channel beam propagates closer to axis *X* and should run across AOC. To direct it across the side facets, two prisms PR1 and PR2 must be attached to AOC. They may be made of the same crystal material with the same crystal orientation. Shapes of the prisms should meet some additional requirements, in particular, parallel propagation of input and output beams and minimal aberrations. Below, several equations are derived for prisms angles satisfying these demands. For clarity, the drawings and further calculations are given for the most popular uniaxial crystal TeO_2 and typical $e \rightarrow o$ wide-aperture diffraction in *XZ* plane.

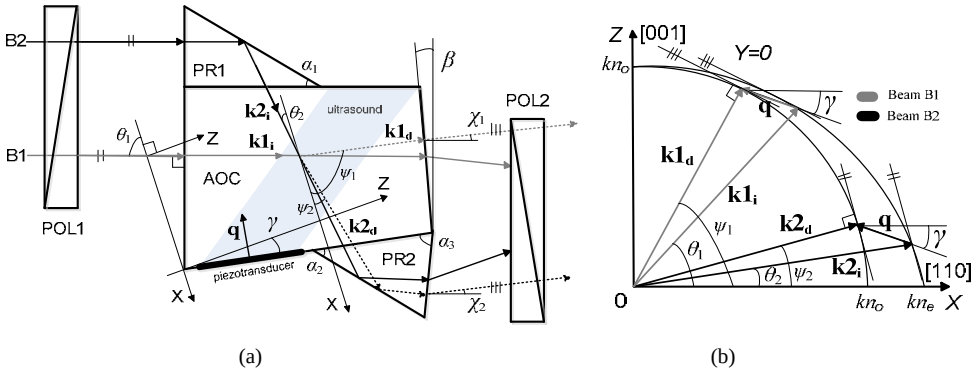

(a) (b)

Fig. 2. Proposed scheme of single-volume dual-channel prism-based AOTF (a) and wave vector diagram (b) in the non-critical phase matching geometry $e \rightarrow o$ anisotropic diffraction.

The first condition satisfies the demand for both input beams to be parallel while the input facets of prism PR1 and AO cell are aligned. In this case,

$$\alpha_1 = (\theta_1 - \theta_2) / 2, \tag{1}$$

where θ_1 and θ_2 are incident light angles corresponding to the condition of wide-aperture AO interaction [13,15]. The output beams directions are defined by the exit face wedge angle β, refractive index n_o and prism PR2 angles α_2 and α_3

$$\chi_1 = \beta + \arcsin\left(n_o \sin\left(\psi_1 - \theta_1 - \beta\right)\right), \tag{2}$$

$$\chi_2 = \arcsin\left(n_o \sin\left(\pi - 2\alpha_2 - \alpha_3 - \psi_2 - \gamma\right)\right) + \alpha_3 - \gamma - \theta_1 \tag{3}$$

To provide parallel propagation of filtered beams after AOTF (i.e. $\chi_1 = \chi_2$), the angle α_2 should match the condition:

$$\alpha_2 = \pi/2 - 1/2\left\{\gamma + \alpha_3 + \psi_2 + \arcsin\left[n_o^{-1} \sin\left(\gamma + \theta_1 - \alpha_3 + \chi_1\right)\right]\right\}. \tag{4}$$

The prism PR2 angle α_3 and AOC angle β may be optimized for the minimization of image chromatic drift [11]. If we additionally require the parallel propagation of the beams B1 and B2 before and after AOTF (i.e. $\chi_1 = \chi_2 = 0$), the angle β has a unique value, which may be obtained from (2):

$$\beta = \arctan\left(\frac{n_o \sin(\psi_1 - \theta_1)}{n_o \cos(\psi_1 - \theta_1) - 1} \right). \quad \textbf{(5)}$$

To complete calculations and design the proposed AOTF, one needs to specify the material and the cut angle γ of AO cell. Then the pair of incident angles θ_1 and θ_2 corresponding to non-critical phase matching condition for extraordinary-polarized incident beams ($e \rightarrow o$) can be found from the equation [15]:

$$\gamma = \operatorname{atan}\left(\frac{\xi \tan\theta}{\sqrt{\left(\xi^4 \tan^2\theta + 1\right)\left(\xi^2 \tan^2\theta + 1\right)} + \xi^3 \tan^2\theta} \right), \quad \textbf{(6)}$$

where $\xi = n_e / n_o$ characterizes the material birefringence. Then the angles of diffracted light propagation ψ_1 and ψ_2 inside the crystal are defined by the expression

$$\psi = \operatorname{atan}\left(\xi^2 \tan\theta\right). \quad \textbf{(7)}$$

3. Setup modelling and optimizing

For the experiments, we used a conventional AOC made of TeO_2 crystal with cut angle $\gamma = 7°$ and back facet angle $\beta = 2.29°$ optimized for chromatic image drift minimization. The input aperture is 9 mm in diameter and piezotransducer length is 12 mm. By applying acoustic frequency in the range 56-145 MHz, this AOTF may be tuned in the wavelength range 450-850 nm. Its bandwidth is 3.5 nm at $\lambda = 532$ nm (140 cm^{-1}).

As we can see from (6), in $e \rightarrow o$ diffraction geometry, the non-critical phase-matching is satisfied in this AOC for light beams propagating at the angles $\theta_1 = 73.85°$ and $\theta_2 = 6.75°$. Using equations (1)-(3), (5) and (7), we have calculated the angles of the prisms PR1 ($\alpha_1 = 33.55°$) and PR2 ($\alpha_2 = 41.67°$), which enable parallel propagation of the filtered beams B1 and B2 at $\chi_1 = \chi_2 = 1.4°$. Angle $\alpha_3 = 81.77°$ was selected for aberration minimization using software Zemax [11]. Diameters of beams B1 and B2 are equal (9 mm) as well as angular apertures (4°×4°).

The total optical scheme of the stereoscopic imager based on the proposed dual-channel prism-based AOTF is depicted in Fig. 3. Objective OBJ ($f_{OBJ} = 50$ mm) forms stereoscopic images of the sample S. Identical lenses L1 and L2 ($f_L = 35$ mm) focus light inside the working volume of AO cell (acoustic beam) and enable confocal diffraction mode [17]. Diaphragms IRIS1 and IRIS2 are located in the front focal planes of L1 and L2 to limit the angular aperture of the beams and to provide telecentric beam propagation in AOC. Prisms PR1 and PR2 provide effective Bragg diffraction of the beam B2 and its propagation after filtration parallel to beam B1. Crossed polarizers POL1 and POL2 are necessary to select diffracted beams. Identical lenses L3 and L4 ($f_L = 35$ mm) focus filtered light beams onto the CMOS monochrome image sensors IM1 and IM2 (Sony IMX273LLR, 1/2.9″, 1440×1080 pixels).

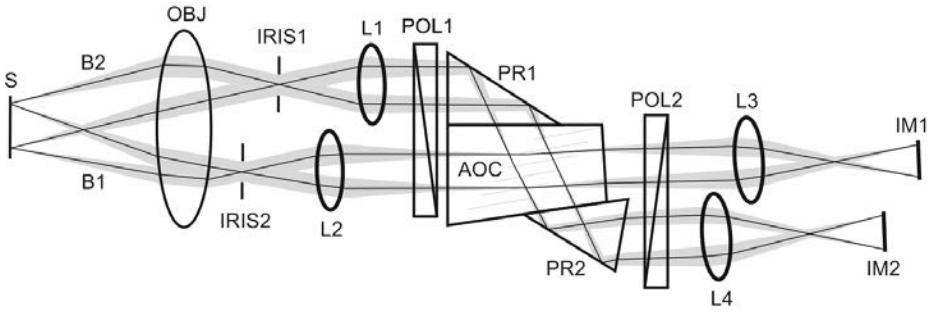

Fig. 3. Optical scheme of the stereoscopic imager based on the single-volume dual-channel prism-based AOTF.

To ensure high-quality spectral images in this scheme, we simulated and optimized it using Zemax software. To take into account image distortion introduced by AOC, we used a ray-tracing AOTF model [11]. As the spectral image shift is inevitable in a single-crystal AOTF configuration, we compensated it for only the central wavelength 600 nm of the AOTF tuning range by proper orientation of the image sensors IM1 and IM2. Residual spectral drift causes slight decrease of the spatial resolution at the edges of the spectral range. Other aberrational parameters were minimized for the whole tuning range 450-850 nm. Results of system optimization are presented in Fig. 4. The maximal spot size does not exceed 25 μm within the whole spectral range that corresponds to 7 pixels of the image sensor.

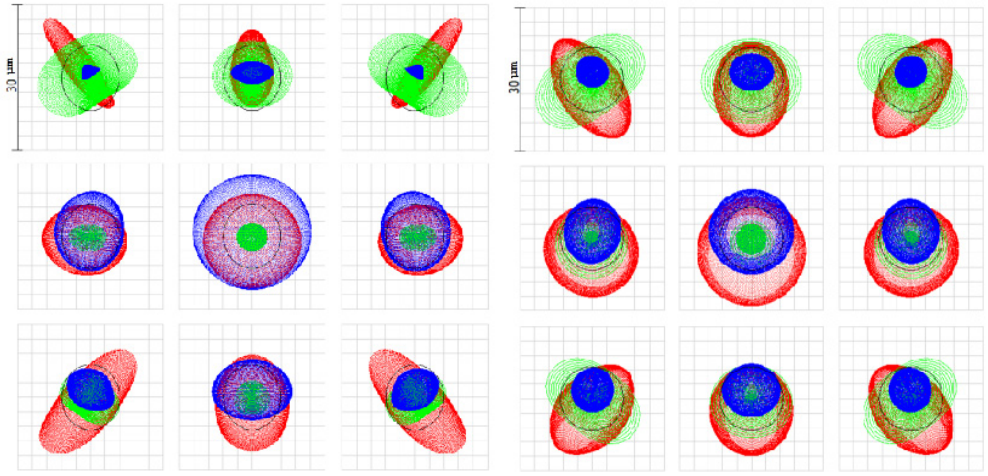

(a) (b)

Fig. 4. Spot diagrams in the center and on the edges of spectral images formed by the beams B1 (a) and B2 (b) at 450 nm (blue), 600 nm (green) and 850 nm (red).

4. Experimental results

To estimate the image quality provided by the designed system, we recorded spectral images of a standard flat test-chart in both channels of the AOTF-based imager. As can be seen in Fig. 5, spatial distortion is barely visible. The spatial resolution is rather high (15 1ines/mm), but is lower than estimated value presumably due to non-ideality of optical components and due to neglecting the divergence and attenuation of the ultrasonic wave, non-uniform crystal heating and other physical factors affecting negatively the image quality.

To illustrate the applicability of the proposed approach for stereoscopic spectral imaging, we compiled the hyperspectral data cubes of various objects. Spectral images at different wavelengths demonstrate significant variations of the spectral contrast of the object (Fig. 6).

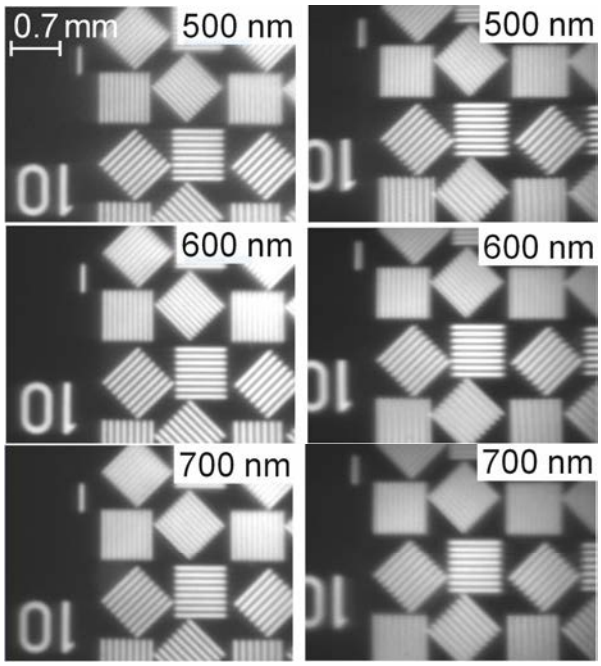

Fig. 5. Spectral stereoscopic images of the test-chart.

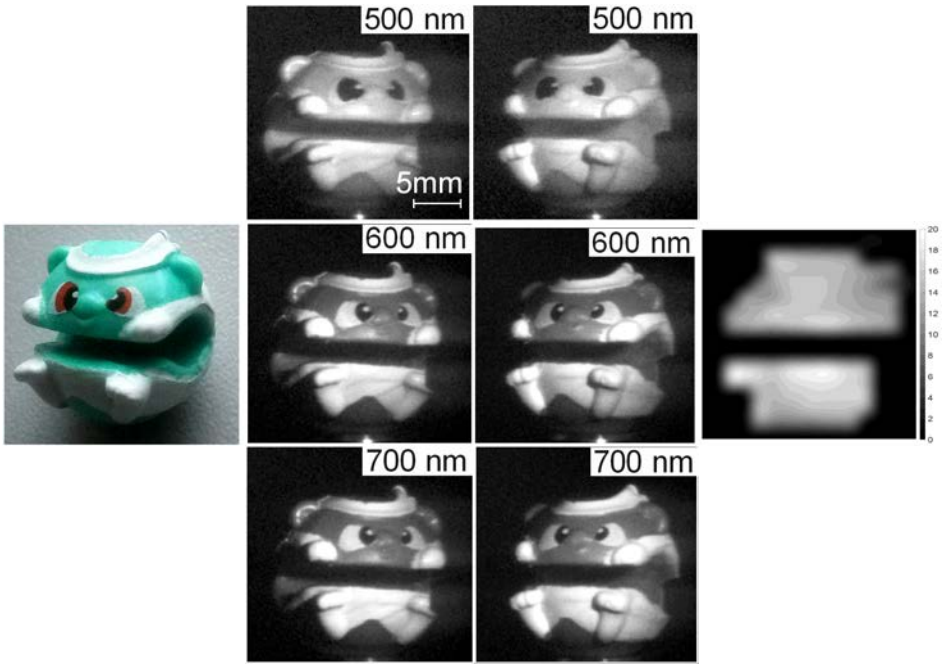

(a) (b) (c) (d)

Fig. 6. Color (a) and spectral stereoscopic (b and c) images, disparity map in pixels at λ = 600 nm (d).

Pair images represent the object in two different orientations, providing stereoscopic view. The depth of scene can be characterized by the disparity map, which displays the coordinates difference in pixels of similar features within stereo images pair [18]. It is usually computed

as a two-dimensional array of such differences. Fig. 6d shows disparity map at λ = 600 nm. Reconstruction of 3D object shape from spectral images is possible by standard processing procedures (rectification, matching, etc.) provided accurate geometrical calibration of the imager [8,15].

5. Conclusion

In this paper, we have presented a new approach to tunable spectral filtration of image-carrying stereoscopic beams. It is based on simultaneous wide-aperture AO diffraction of two beams via single acoustic wave. In general, such single-volume geometry requires a tricky shaped large AO cell or complicated optical relay system. To overcome these drawbacks, we propose to attach to ordinary wide-aperture AO cell a pair of triangular prisms of the same material. They enable effective AO filtration of the second beam and provide output filtered beams to be parallel to the incident beams that is very important for practical implementations.

Developed device is free of moving elements and is fully PC-controlled, provides arbitrary spectral access, performs high-contrast spectral imaging and enables calculating 3D shape of the inspected object. Using previously developed AOTFs' configurations and the proposed approach one can design a variety of new spectral elements for stereoscopic spectral imaging with spectral parameters (range and resolution) to satisfy particular application requirements.

Funding

This research is supported by Russian Science Foundation (project 19-19-00606).

Disclosures

The authors declare no conflicts of interest.

References

1. D. Manolakis, R. Lockwood and T. Cooley, "Hyperspectral Imaging Remote Sensing: Physics, Sensors, and Algorithms," Cambridge University Press, 2016. 706 p.
2. N. Basantia, L. Nollet and M. Kamruzzaman, "Hyperspectral Imaging Analysis and Applications for Food Quality," CRC Press, 2018. 284 p.
3. T. Bourlai, "Face Recognition Across the Imaging Spectrum," Springer, 2016. 383 p.
4. J. Geng, "Structured-light 3D surface imaging: a tutorial" Adv. in Opt. and Phot. **3**(2), 128-160 (2011).
5. H. Zhao, L. Xu, S. Shi, H. Jiang and D. Chen, "A High Throughput Integrated Hyperspectral Imaging and 3D Measurement System," Sensors, **18**(4), 1068 (2018).
6. S. Yoon and C. Thai, "Stereo spectral imaging system for plant health characterization," Proc. ASABE Annual Int. Meeting, 096583 (2009).
7. H. Zhao, S. Shi, H. Jiang, Y. Zhang and Z. Xu, "Calibration of AOTF-based 3D measurement system using multiplane model based on phase fringe and BP neural network," Opt. Exp. **25**(9) 10413-10433 (2017).
8. S. Zhang, "Handbook of 3D Machine Vision: Optical Metrology and Imaging." 1st Edition, CRC Press, 2017. 414 p.
9. C. Tran, "Acousto-optic tunable filter: A new generation monochromator and more," Analyt. Lett. **33**(9), 1711-1732 (2000).
10. G. Lu and B. Fei, "Medical hyperspectral imaging: a review," J. Biomed. Opt., **19**(1), № 010901 (2014).
11. A. Machikhin, V. Batshev and V. Pozhar, "Aberration analysis of AOTF-based spectral imaging systems," JOSA A, **34**(7), 1109-1113 (2017).
12. A. Machikhin, V. Batshev, V. Pozhar and M. Mazur, "Acousto-optical full-field stereoscopic spectrometer for 3D reconstruction in arbitrary spectral intervals," Comp. Opt., **40**(6), 871-877 (2016).
13. V. Epikhin, F. Vizen and L. Paltsev, "Acousto-optic filtration of light with arbitrary polarization," Tech. Phys., **57**(10), 1910-1914 (1987).
14. V. Voloshinov, V. Molchanov and T. Babkina, "Acousto-optic filter of nonpolarized electromagnetic radiation," Tech. Phys., **45**(9), 1186–1191 (2000).
15. A. Machikhin, V. Batshev, V. Pozhar, A. Naumov and A. Gorevoy, "Acousto-optic tunable spectral filtration of stereoscopic images," Opt. Lett., **43**(5), 1087-1090 (2018).
16. A. Machikhin and V. Pozhar, "Obtaining Spectral Stereo Images with Electron Spectral Tuning and Polarization Separation," Tech. Phys. Lett., **40**(9), 823–826 (2014).
17. D. Suhre, L. Denes and N. Gupta, "Telecentric confocal optics for aberration correction of acousto-optic tunable filters," App. Opt., **43**(6), 1255-1260 (2004).
18. L. Shapiro and G. Stockman, "Computer Vision," Prentice Hall, 2001. 608 p.